Applied Surface Science 572 (2022) 151397

Contents lists available at ScienceDirect

Applied Surface Science

journal homepage: www.elsevier.com/locate/apsusc

Full Length Article

Sequential growth of self-organized epitaxial $FeSi_2$ and $CoSi_2$ nanostructures on Si(1 1 1)-7 × 7 surfaces

J.C. Mahato [a,b,*], Debolina Das [c], Arindam Pal [d], Prabir Pal [e,f], B.N. Dev [g]

[a] Department of Physics, Ramakrishna Mission Residential College (Autonomous), Narendrapur, Kolkata 700103, India
[b] Institute of Applied Physics, Technical University of Braunschweig, Braunschweig 38106, Germany
[c] Department of Physics, Haldia Government College, Haldia, Debhog 721657, India
[d] Department of Physics, Yogoda Satsanga Palpara Mahavidyalaya, Palpara, Purba Medinipur 721458, West Bengal, India
[e] Energy Materials and Devices Division, CSIR-Central Glass and Ceramic Research Institute, 196, Raja S.C. Mullick Road, Kolkata 700 032, India
[f] Academy of Scientific and Innovative Research (AcSIR), Ghaziabad 201002, India
[g] Centre for Quantum Engineering, Research and Education (CQuERE), TCG Centres for Research and Education in Science and Technology, Tower 1, Bengal Eco Intelligent Park (Techna Building), Block EM, Sector V, Salt Lake, Kolkata 700091, India

ARTICLE INFO

Keywords:
Self-organized epitaxial silicides
Reactive deposition epitaxy
Nanodots and nanowires
Scanning tunneling microcopy

ABSTRACT

Epitaxial γ-$FeSi_2$ and $CoSi_2$ nanostructures, grown on a vicinal Si(1 1 1)-7 × 7 surface by sequentially depositing 1-monolayer (ML) of Fe and 1ML of Co on a hot Si substrate under ultrahigh vacuum condition, have been investigated by in-situ scanning tunneling microscopy, ex-situ field emission scanning electron microscopy and x-ray photoemission spectroscopy (XPS). While γ-$FeSi_2$ nanostructures have grown as nanowires along the three equivalent ⟨1 1 0⟩ directions on the Si(1 1 1) surface, $CoSi_2$ nanoislands have grown as equilateral triangular and trapezoidal islands. Such self-organized nanostructures may find applications in nanoscale devices including S-F hybrids for quantum technology, as $CoSi_2$ is a superconductor (S) and γ-$FeSi_2$ is a ferromagnet (F).

1. Introduction

The transition metal silicides, especially chromium disilicide, manganese disilicide, iron disilicide, cobalt disilicide, nickel disilicide etc. are very important active components of nanoelectromechanical devices due to their very special mechanical [1–5], thermal [1,2,4], optical [3,6-10], electrical [3,7] and magnetic [6,11-20] properties. These silicides are very useful in the nanodevices because of their high thermal stability nearly up to ~ 1000 °C, and they form very sharp interface with the substrate and the Schottky barrier height can be tuned by proper choice of silicide material [1,2,4]. Among these metal silicides, iron disilicide ($FeSi_2$) and cobalt disilicide ($CoSi_2$), are two most important silicides. For nanoelectronics, it is important to understand the silicide/silicon systems in the nanoscale [18-22].

Another potential development would arise from the fact that $CoSi_2$ is a superconductor, in the bulk form [23,24] as well as in epitaxial structures on silicon [25,26], and γ-$FeSi_2$ is a ferromagnet [27-30]. Bulk $CoSi_2$ has a superconducting transition temperature (T_C) of ~ 1.4 K [23], very similar to that of aluminum (T_C = 1.2 K)- a popular material for making superconducting quantum circuits [31]. The intrinsically low noise properties of superconducting epitaxial $CoSi_2$ thin films on Si, even compared to aluminum, could be utilized for developing quiet *qubits* and scalable superconducting circuits for future quantum computing [26]. We have earlier grown epitaxial $CoSi_2$ [32-34] and γ-$FeSi_2$ [35] individually on silicon substrates. However, growing γ-$FeSi_2$ and $CoSi_2$ nanostructures together on a single substrate assumes importance in view of the application of ferromagnet-superconductor hybrids (FSH) in quantum technology [36]. The so-called FSHs are spatially separated but closely located ferromagnets and superconductors. In general, many different kinds of hybrid systems are the candidates for the development of quantum technologies. Hybrid quantum systems composed of different physical components with complementary functionalities may provide multi-tasking capabilities [37]. Epitaxial growth of both $FeSi_2$ and $CoSi_2$ nanostructures on the same silicon substrate may lead to the integration of the relevant quantum technologies with the well-established silicon technology.

Numerous research groups have widely investigated the growth of self-organized epitaxial $FeSi_2$ nanostructures on Si(1 1 1)-7 × 7 surfaces [11,38-44]. Also there are reports on the growth of self-organized epitaxial $CoSi_2$ on the Si(1 1 1)-7 × 7 surfaces [22,45-50]. But there is

* Corresponding author.
E-mail addresses: jagadishchmahato4@gmail.com, j.mahato@tu-braunschweig.de (J.C. Mahato).

https://doi.org/10.1016/j.apsusc.2021.151397
Received 10 July 2021; Received in revised form 15 September 2021; Accepted 22 September 2021
Available online 25 September 2021

no report on the epitaxial growth of more than one silicide on the same Si(1 1 1)-7 × 7 surfaces. Also there is no investigation on how Co reacts when it is deposited on the hot Si(1 1 1)-7 × 7 surfaces which are pre-decorated with $FeSi_2$ nanostructures. In other words, there is no report on the influence of one silicide (here, $FeSi_2$) nanostructures on the growth of another silicide on the same Si(1 1 1)-7 × 7 surfaces. In this article an attempt has been made to address this issue. Growth of more than one silicide may play a significant role if the device fabrication via self-organized growth process can be realized in future. In this paper, for the first time we present the fabrication of concomitant self-organized epitaxial $FeSi_2$ NWs and $CoSi_2$ nanodots or nanoislands on 3°-miscut vicinal Si(1 1 1)-7 × 7 surfaces. The detailed morphology of the $FeSi_2$ and $CoSi_2$ nanostructures has been investigated by *in-situ* scanning tunneling microscopy (STM) measurements and ex-situ field emission scanning electron microscopy (FE-SEM) measurements. The formation of the two distinct disilicides has been confirmed by X-ray photoelectron spectroscopy (XPS) measurements.

2. Experimental

Atomically clean 3°±0.1° vicinal Si(1 1 1)-7 × 7 surfaces were prepared by degassing the substrate at ~ 700 °C for 14–16 h and then flashing the sample at ~ 1250 °C for one min under ultrahigh vacuum (UHV) environment (~5 × 10^{-10} mbar) in a molecular beam epitaxy (MBE) chamber. We raised the substrate temperature to ~ 1250 °C, kept there for one min, and then cooled it down to ~ 870 °C and kept at that temperature for 30 min and then allowed the substrate to attain the room temperature slowly by switching off the sample heating direct current. The clean surface thus prepared possesses atomically flat Si (1 1 1)-7 × 7 surfaces with small terraces. One monolayer (ML) (1ML = 9.59 × 10^{14} atoms/cm^2) of Fe atoms has been deposited on the hot substrate at ~ 600 °C. This method produces γ-$FeSi_2$ [27,28,35]. After *in-situ* STM measurement of the Fe-deposited Si(1 1 1)-7 × 7 surfaces, the $FeSi_2$ decorated surface is transferred to the MBE growth chamber and then heated again to ~ 600 °C to deposit 1.0 ML Co onto it. As the MBE and the STM chambers are interconnected, both under UHV condition, the sample is never exposed to air. The Fe- and Co-deposited Si(1 1 1)-7 × 7 surface was investigated by in-situ STM. Then the sample was taken out of the MBE-STM chamber to perform FE-SEM and subsequently XPS measurements. The XPS measurements were performed by using PHI 5000 VERSAPROBE II, Physical Electronics system equipped with a monochromatic Aluminum K_α (1486.7 eV) high flux focused X-ray source and a multi-channeltron hemispherical electron energy analyzer. All the spectra were collected at an emission angle of 45° with the base vacuum of 4.0 × 10^{-10} mbar. The binding energy calibration was done by measuring C 1 s keeping at 284.6 eV. The total energy resolution, estimated from the width of the Fermi edge, was about 400 meV for monochromatic Aluminum K_α line with pass energy 11.750 eV. A charge neutralizer was utilized in order to compensate the surface charging of the samples.

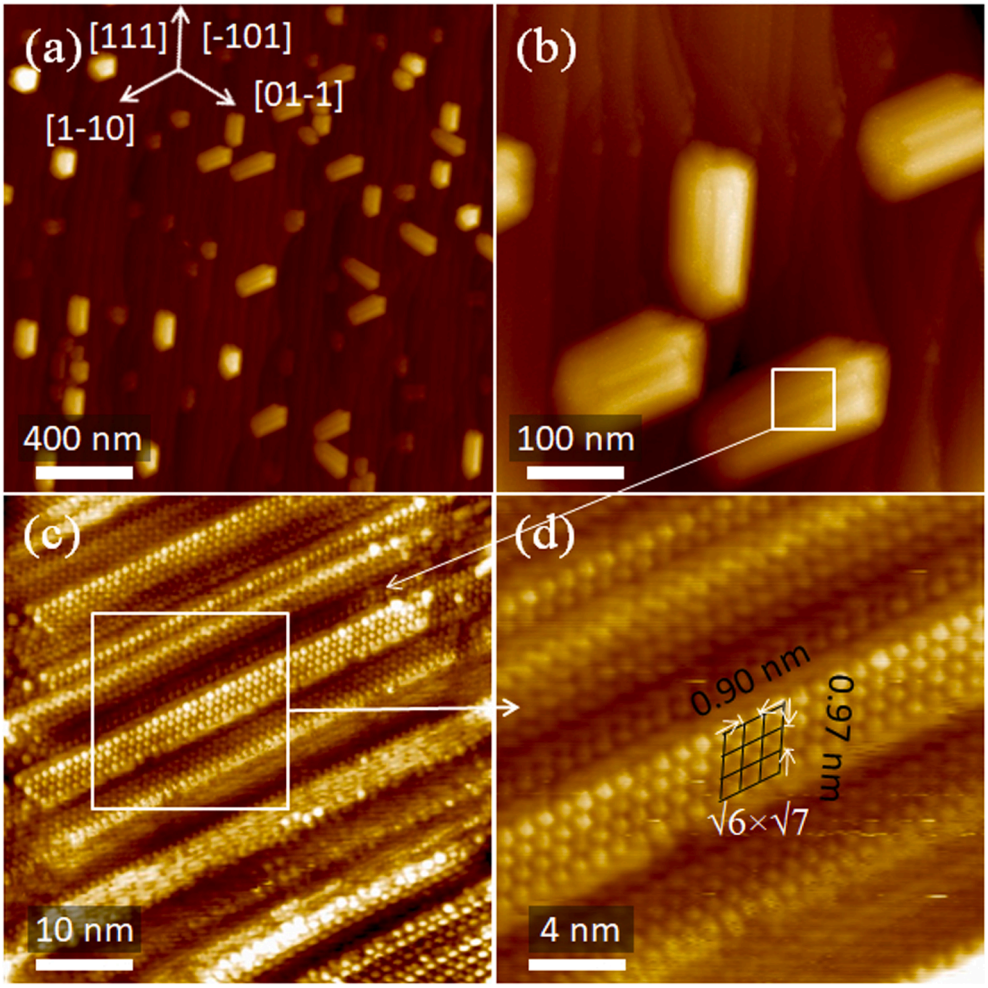

Fig. 1. Fig. (a-d) show the STM images of the $FeSi_2$nanowires grown as a result of 1.0 ML Fe deposition on the Si(1 1 1)7 × 7 surfaces at ~ 600 °C. The filled state (V_g = -1.6 V and I_t = 0.2nA) STM images show the atomic arrangement of the top surface of the $FeSi_2$ atomic rows.

3. Results and discussion

3.1. Self-organized epitaxial $FeSi_2$ nanostructures on Si(1 1 1)-7 × 7 surfaces via reaction deposition epitaxy

STM images of an atomically clean 3°-miscut vicinal Si(1 1 1) surface, recorded at a bias voltage, $V_g = 1.9$ V and tunneling current, $I_t = 0.2$nA, have shown typical (7 × 7) surface reconstruction on the terraces; the average terrace width of this vicinal clean surface is ~ 50 nm (not shown here). Fig. 1 shows STM images of the $FeSi_2$nano-islands grown on the 3°-miscut vicinal Si(1 1 1)-7 × 7 reconstructed surface, recorded at a bias voltage V_g = -1.6 V and tunneling current, I_t = 0.2nA. The heights of the nano-islands lie in the range from 8.5 to 14.0 nm. The $FeSi_2$nano-islands are elongated along three in-plane ⟨1 1 0⟩ crystallographically equivalent directions. The atomic resolution STM image on the top surfaces of these $FeSi_2$nano-islands shows well-ordered atomic arrangements on stripe-like structures (Fig. 1(c, d)). On relatively wider stripes, the unit cell shows a $(\sqrt{6}\times\sqrt{7})$ reconstruction, as shown in Fig. 1(d). Fig. 2(a- d) shows the magnified images of a single $FeSi_2$nanowire. Fig. 2(a) is the STM image recorded at bias voltage, V_g = 1.6 V, tunneling current I_t = 0.2nA and Fig. 2 (b) is the current image of the former. From Fig. 2(a, c), the Si(1 1 1)7 × 7 reconstruction is clearly visible surrounding the $FeSi_2$nanowire. This indicates Volmer-Weber growth of $FeSi_2$. The different facets of the pyramid shaped nano-island of $FeSi_2$ possess different surface atomic arrangements as seen from Fig. 2(c-d). The nature of the $FeSi_2$nanowires here are different from those on Si(1 1 0) surfaces [35]. The $FeSi_2$nanowires in Ref. 35, possess comb-like structures on the two side walls, which could be related to the (16 × 2) reconstruction on the Si(1 1 0) surface, and all the nanowires grow along one direction because of the twofold symmetry of the Si(1 1 0) surface. Here the $FeSi_2$nanowires grow along the three ⟨1 1 0⟩ in-plane directions, due to the threefold symmetry of the Si(1 1 1) surface, and they do not show comb-like features.

3.2. Self-organized epitaxial $CoSi_2$ and $FeSi_2$ nanostructures on Si(1 1 1)-7 × 7 surfaces via reaction deposition epitaxy

Fig. 3 (a, c) show the STM images of the $FeSi_2$ and $CoSi_2$ nanostructures grown on Si(1 1 1)-7 × 7 surfaces. Fig. 3(b, d) show the current images of the corresponding STM images in Fig. 3(a, c). Comparing the morphology of the nanostructures of these Fe- and Co-deposited surface with that of only Fe-deposited surface, it is evident that triangular and trapezoidal nanostructures have appeared (encircled in Fig. 3(a, c)), in addition to those which had already grown on the surface when only Fe was deposited. Current image of Fig. 3(c) in Fig. 3(d) clearly shows the triangular and trapezoidal nanostructures and also the nanowires. The current image (derivative mode) displays enhanced information when the z-scale varies fast. Here, we can see this feature of the sidewall facets of the silicide nanowires and nanoislands more prominent in Fig. 3(b, d). The edges of the triangular and the trapezoidal islands are along the

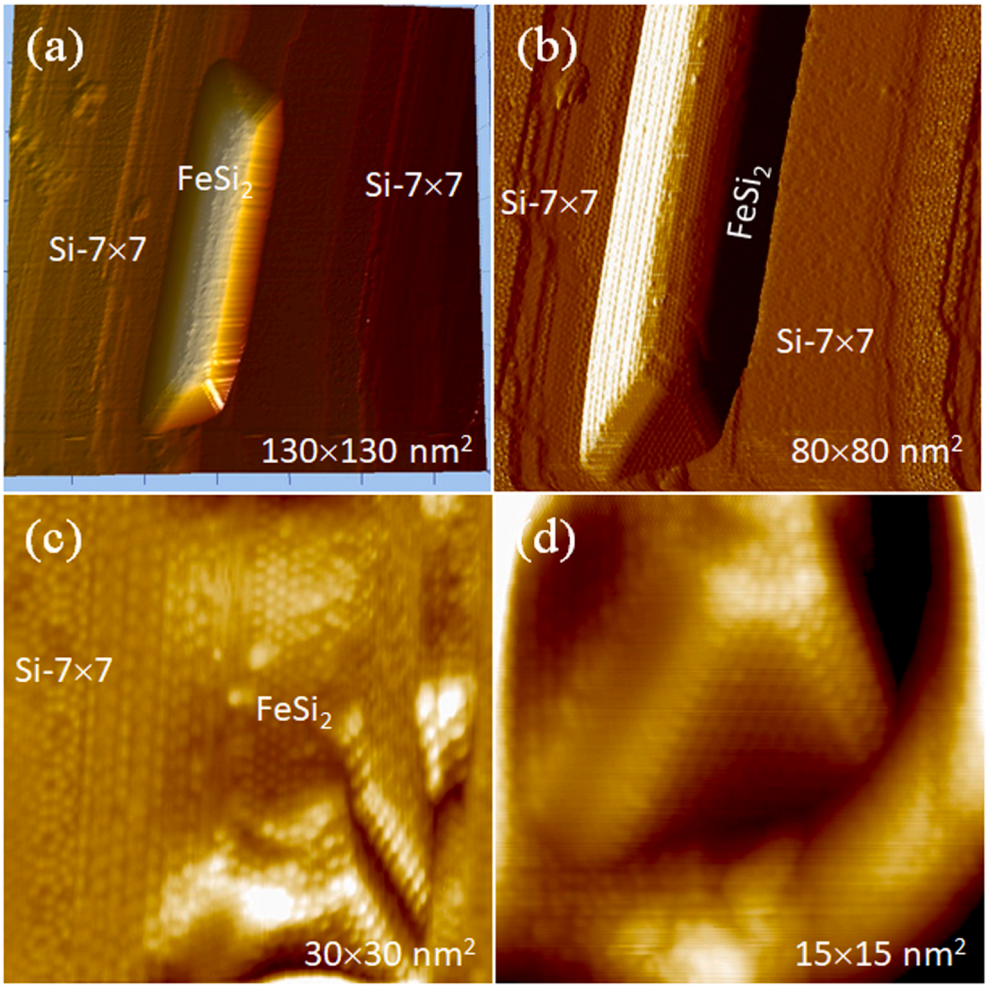

Fig. 2. (a) shows the 3D view of the STM image of a $FeSi_2$ NW grown on Si(1 1 1)-7 × 7 clean surfaces. (b) shows the current image of the STM image of the same FeS_2 NW. Surrounding the NW, the 7 × 7 reconstruction is sustained. (c, d) show the atomically resolved STM images of the NW. Different facets of the NW show different atomic arrangements.

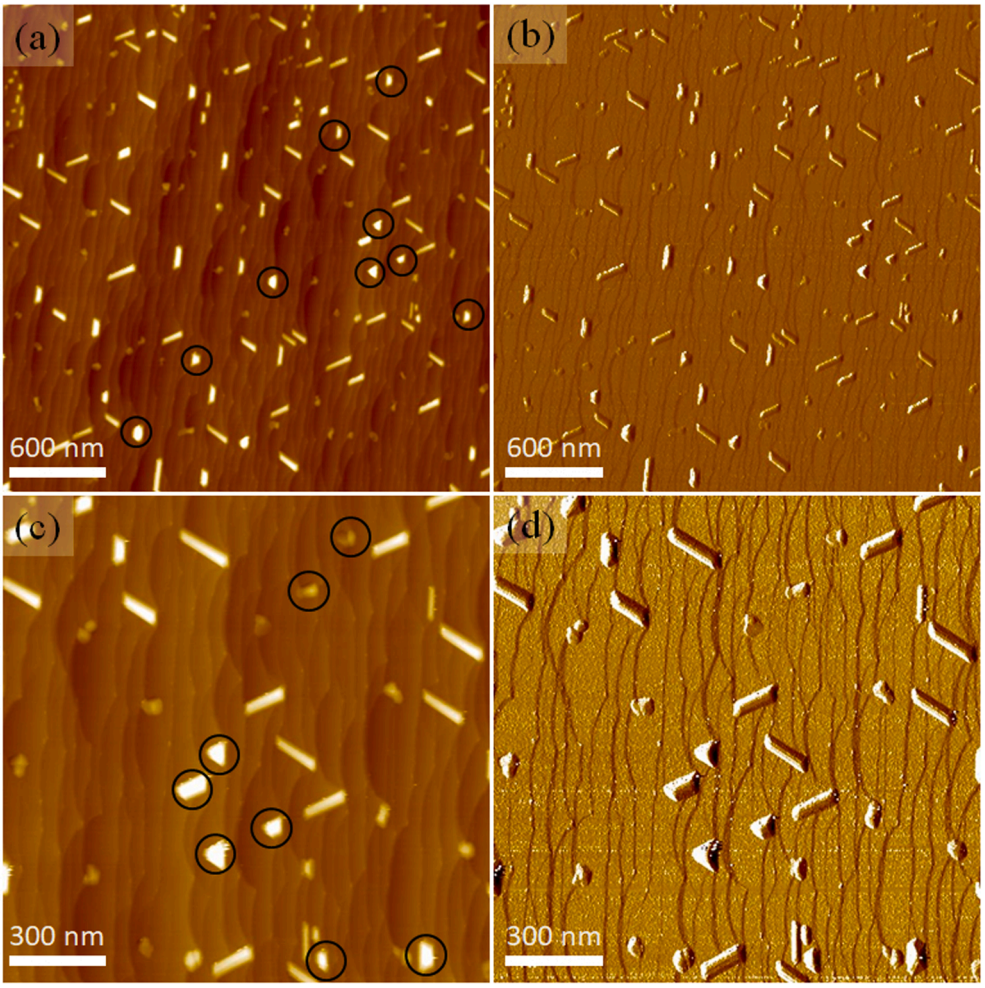

Fig. 3. (a) and (c) show the STM images (bias voltage, $V_g = 1.9$ V and tunneling current, $I_t = 0.2$nA) of the $FeSi_2$ and $CoSi_2$ NWs and nanostructures grown on the Si (1 1 1)-7 × 7 surface. (b, d) show the current images of the STM images shown in (a) and (c) respectively.

three in-plane ⟨1 1 0⟩ crystallographically equivalent directions. For $CoSi_2$ growth on Si(1 1 1)-7 × 7 surfaces, these growth features have earlier been observed [32,48]. From Fig. 3(a) we notice that the trapezoidal islands are preferentially aligned along the step edges – a feature observed in other cases of epitaxial island growth on vicinal Si(1 1 1) surfaces [50,51].

Fig. 4(a-d) shows the STM image of $FeSi_2$ NWs and $CoSi_2$ nanostructures grown on the vicinal Si(1 1 1)-7 × 7 surface. Fig. 4(b) shows the magnified image of marked part in (a). Fig. 4(c) shows the three-dimensional view of the nanoisland in the upper part seen in (b) and (d) is its current image. The nanoisland possesses five distinct side facets. The high resolution STM image reveals that there are different atomic arrangements on these side facets.

Fig. 5 shows the STM image of a flat terrace silicide island in (a-c). Fig. 5(c) shows the 2 × 2 reconstructed atomically resolved STM image of the top surface of the silicide island of the box marked location in (b). Fig. 5(d) is the Fast Fourier transform (FFT) image of Fig. 5(c). The unit cell dimension of the FFT image is 1.31 nm^{-1}, which corresponds to the direct lattice unit cell of side 0.76 nm.

SEM investigation also supports the STM morphology investigation. Fig. 6 shows the SEM image recorded at 5.0 kV. In Fig. 6, the $FeSi_2$ nanowires have been marked as 'F' and the $CoSi_2$ triangular islands have been marked as 'C' in the SEM image. Though, the nanowires are mainly made up of $FeSi_2$, it is to be worth mentioned that out of the nanowires as seen in the STM as well as SEM images, there may be a very few $CoSi_2$ nanowires too. As it is reported earlier, deposition of cobalt on the Si (1 1 1)-7 × 7 results in the formation of triangular as well as a very few cobalt disilicide nanowires with them [45,48]. The line profile plot on the $FeSi_2$ and $CoSi_2$-grown sample reveals that the compact nanoislands are taller than the elongated nanowires. The height of the nanodots lies in the range of 25.0–30.0 nm whereas the height of the nanowires lies in the range of 8.5–14.0 nm from the substrate surface. The line profile on the top left insets of Fig. 4(b) has been measured on the nanoislands and that on the top right inset of Fig. 4(b) has been measured on the nanowires.

Let us try to understand the difference between the shapes of $CoSi_2$ and γ-$FeSi_2$ islands. $CoSi_2$ islands grow predominantly as equilateral triangular structures on the threefold symmetric Si(1 1 1) substrate. Earlier, gold-silicide islands were also found to grow on Si(1 1 1) as equilateral triangular structure up to a critical size; islands larger than the critical size undergoes a shape transition to trapezoidal islands [51]. We observe both equilateral and trapezoidal $CoSi_2$ islands in the present case. It is to be noted that shape transition of $CoSi_2$ islands on Si(1 0 0), which is fourfold symmetric, is from square-shaped islands to rectangular islands beyond the critical size; rectangular islands can grow into very long nanowires [33]. There are no such reported results for γ-$FeSi_2$ on Si(1 1 1) substrates. Here we observe that even the smallest γ-$FeSi_2$ islands appear to be elongated and the nanowires have grown along the three equivalent ⟨1 1 0⟩ directions. Logically, the longer edge of the trapezoidal $CoSi_2$ islands also should be aligned along the three equivalent ⟨1 1 0⟩ directions. However, earlier studies of epitaxial growth on stepped Si(1 1 1) surfaces have shown that the trapezoidal islands

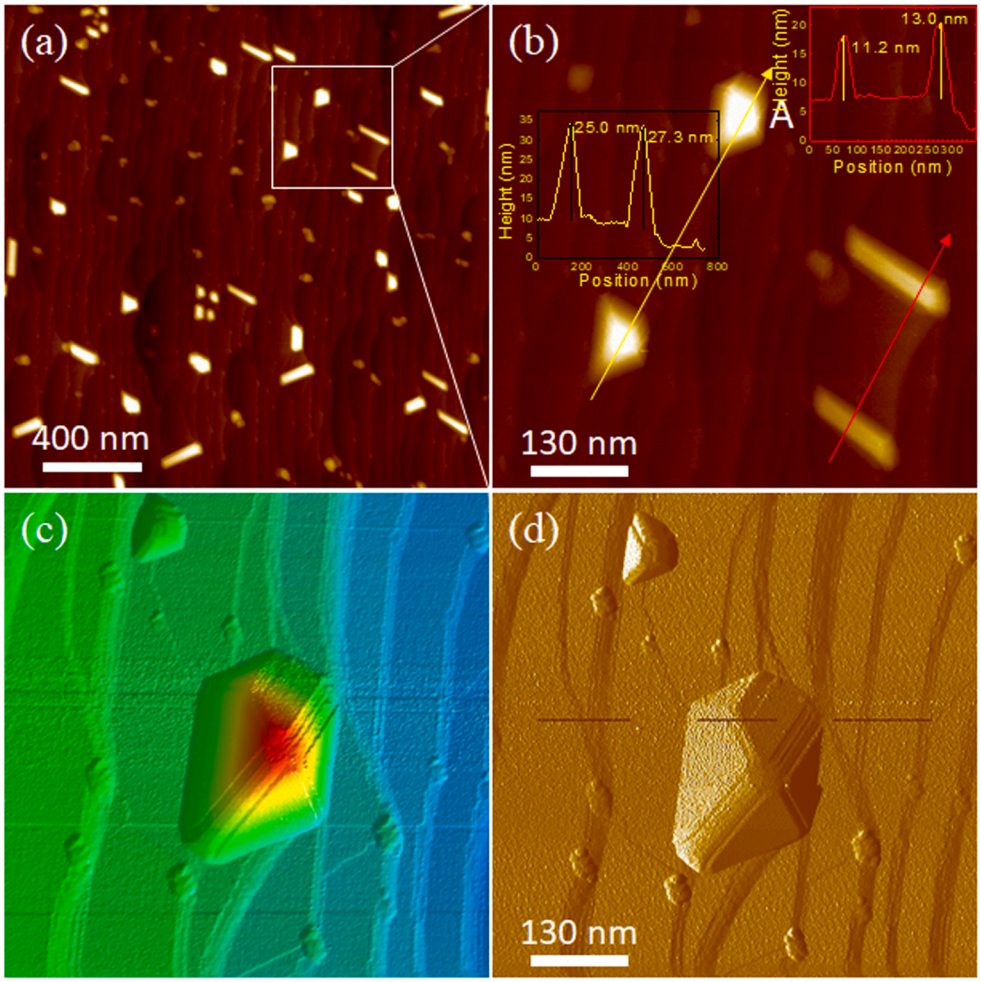

Fig. 4. (a-d) shows the STM images (bias voltage, $V_g = 1.5$ V and tunneling current, $I_t = 0.2$nA) of $FeSi_2$ and $CoSi_2$ NWs and nanostructures on the Si(1 1 1)-7 × 7 surface. Fig. 4 (b) shows a magnified image of the boxed part of (a). Fig. (c) shows the three-dimensional view of the nanoisland marked 'A' in the upper part in (b). (d) is the current image of its corresponding STM image, clearly displaying the distinct facets of the nanoisland.

preferentially grow along the step edges [50], as observed here. We believe that the difference in the observed shape of $CoSi_2$ and γ-$FeSi_2$ islands is related to the interface structure of these two systems. To our knowledge, no good quality interface structural analysis is available for γ-$FeSi_2$/Si(1 1 1). We can compare the cases of $CoSi_2$/Si(1 1 0) [34] and γ-$FeSi_2$/Si(1 1 0) [35], for which high quality interface analyses are available. The $CoSi_2$/Si(1 1 0) system is a case of simple epitaxy where the interface is simply A- or B-type, [34] as known from many other studies. However, for the γ-$FeSi_2$/Si(1 1 0) system, the interface structure is more complex. It is a case of tilted epitaxy and the resulting interface presents a network of intrinsic interfacial dislocations [35]; this can be understood in terms of generalized heteroepitaxy [52-54]. We believe, the difference of shapes between the $CoSi_2$ and γ-$FeSi_2$ nanostructures arises, at least partially, from their different interface structures.

3.3. X-ray photoelectron spectroscopy (XPS) measurements of the epitaxial $FeSi_2$ and $CoSi_2$ nanostructures on Si(1 1 1)-7 × 7 surface

In Fig. 7, XPS core-level spectra of (a) Co 2p, (b) Fe 2p, (c) Si 2p, and (d) O 1 s, collected from the sample, depicting the co-existence of $CoSi_2$ and $FeSi_2$ formation on the Si(1 1 1) surface. Experimental core-level spectra (open circles) and fitted spectra (red) are plotted together and shifted along the *y*-axis for clarity. (a): Three pairs of components, used to fit the entire Co 2p core-level region, are also displayed. Features belonging to $CoSi_2$, $Co(OH)_2$ and satellites are shown by blue, wine, and navy, respectively. (b): Three pairs of components used to fit the entire Fe 2p core-level region are displayed. Features belonging to $FeSi_2$, FeO and satellites are shown by blue, dark yellow, and navy, respectively. (c): Two pairs of components used to fit the entire Si 2p core-level region are displayed. Features belonging to Si(1 1 1) and (Fe, Co)Si_2 are shown by wine and blue, respectively. (d): Two components used to fit the O 1 s core-level region are displayed. Features belonging to O^{2-} and OH^- are shown by blue and pink, respectively.

We have investigated the Co 2p, Fe 2p, Si 2p and O 1 s core-level spectra, which are shown in Fig. 7(a), 7(b), 8(c) and 7(d), respectively. The Co $2p_{3/2}$ and Co $2p_{1/2}$ spin–orbit doublet peaks are centered at ~ 778.6 eV and ~ 793.6 eV, respectively [55]. The spin–orbit doublet peaks are wide and show two components in each doublet, a lower binding energy pair of peaks which are related to the $CoSi_2$ components and other higher binding energy pair of peaks are related to $Co(OH)_2$ components. We have carefully fitted the spectrum using following fitting parameters for $CoSi_2$ components as shown by blue line shapes: spin–orbit splitting 15.0 eV, branching ratio 2.5, full widths at half maximum (FWHM) 2.6 eV and an integral background being subtracted before fitting. While $Co(OH)_2$ components are shown by wine line shapes obtained by using spin–orbit splitting 15.3 eV, branching ratio 5.0 and FWHM 3.8 eV. The satellite peaks are observed at ~ 7.0 eV above for $CoSi_2$ shown by navy line shapes [55].

The Fe $2p_{3/2}$ and Fe $2p_{1/2}$ spin–orbit doublet peaks are located at around 707 eV and 719.9 eV, respectively with a pair of shake-up

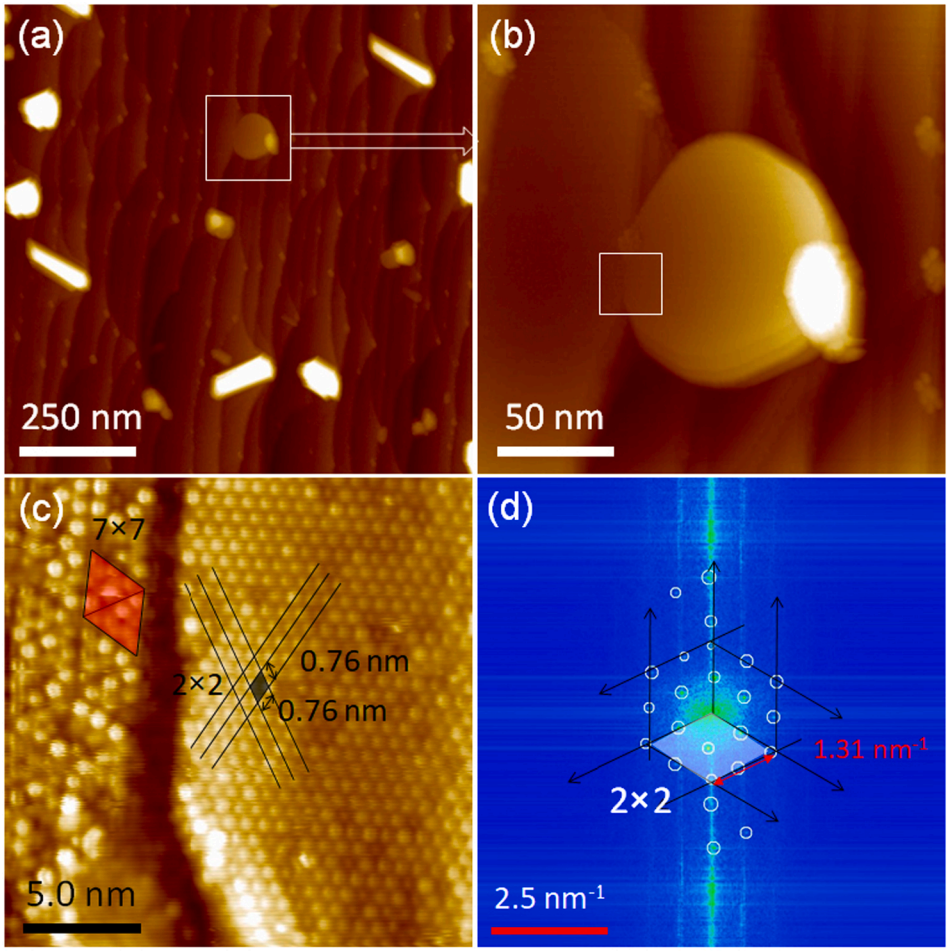

Fig. 5. The STM image shows a flat terrace silicide island in (a-c). (c) shows the 2 × 2- R30° reconstructed atomically resolved STM image of the top surface of the silicide island of the box marked location in (b). (d) is the Fast Fourier transform (FFT) image of (c).

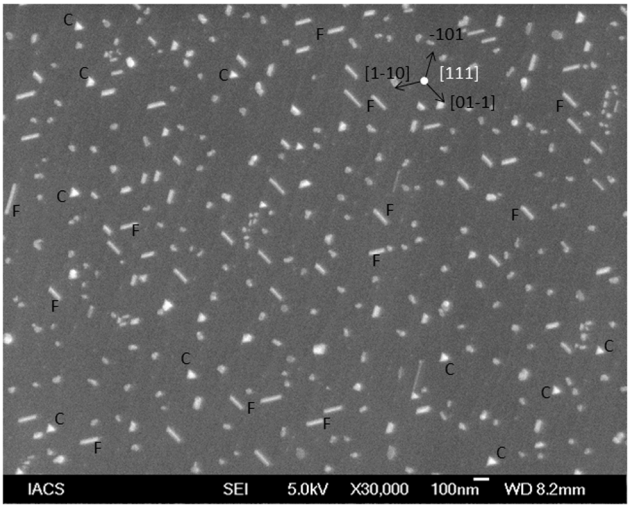

Fig. 6. The SEM image shows the co-existence of $FeSi_2$ nanowires and $CoSi_2$ triangular islands on Si(1 1 1) surfaces. The Nanowires grow predominantly in three crystallographically symmetric in-plane ⟨1 1 0⟩ directions.

satellite peaks located at 8.8 eV above of their spin–orbit doublet peaks [56]. The fitted Fe 2p spectrum highlights characteristic doublet peaks of $FeSi_2$ species at ~ 707.0 eV and ~ 719.8 eV for Fe $2p_{3/2}$ and Fe $2p_{1/2}$, respectively, and doublet peaks of FeO species at ~ 708.3 eV and ~ 721.8 eV for Fe $2p_{3/2}$ and Fe $2p_{1/2}$, respectively. This suggests the presence of $FeSi_2$ and iron(II)-oxide (FeO) at the surface of Si(1 1 1). The presence of Si(1 1 1), $FeSi_2$ and $CoSi_2$ were visible from the characteristics peaks of Si 2p core-level spectrum [56]. The Si $2p_{3/2}$ and Si $2p_{1/2}$ spin–orbit doublet peaks are located at around 99.2 eV and 99.8 eV, respectively corresponding to Si(1 1 1) species. The higher binding shoulders at around 99.4 eV and 100.0 eV for Si $2p_{3/2}$ and Si $2p_{1/2}$, respectively correspond to $FeSi_2$ and $CoSi_2$ species. The presence of O^{2-} and OH^- peaks at ~ 531.6 eV and ~ 532.8 eV, respectively in the O 1s core-level further demonstrates the formation of silicide, oxides/hydroxyl species of cobalt and iron on the surface of Si(1 1 1) as shown in Fig. 7(d). Thus, the spectroscopic investigation showed the formation of cobalt and iron disilicide on Si(1 1 1) [56].

4. Summary and conclusions

Self-organized epitaxial $FeSi_2$ NWs and $CoSi_2$ nano-islands have been grown on the same Si(1 1 1)-7 × 7 surface for the first time. The morphology has been investigated by in-situ scanning tunneling microscopy and field emission scanning electron microscopy. The spectroscopic characteristics of $FeSi_2$ and $CoSi_2$ have been confirmed by x-ray photoelectron spectroscopy measurements. $FeSi_2$ grows as nanowires and $CoSi_2$ grows predominantly as nanoislands. This investigation establishes that $CoSi_2$ nanostructure grows on the exposed Si(1 1 1)-7 × 7 surface of the $FeSi_2$-decorated substrate upon Co deposition. $FeSi_2$ nanostructures remain stable while heating the sample at ~ 600 °C for cobalt deposition. There is no noticeable influence of the pre-existing $FeSi_2$ nanostructures on the Si(1 1 1)-7 × 7 surface. The two types of

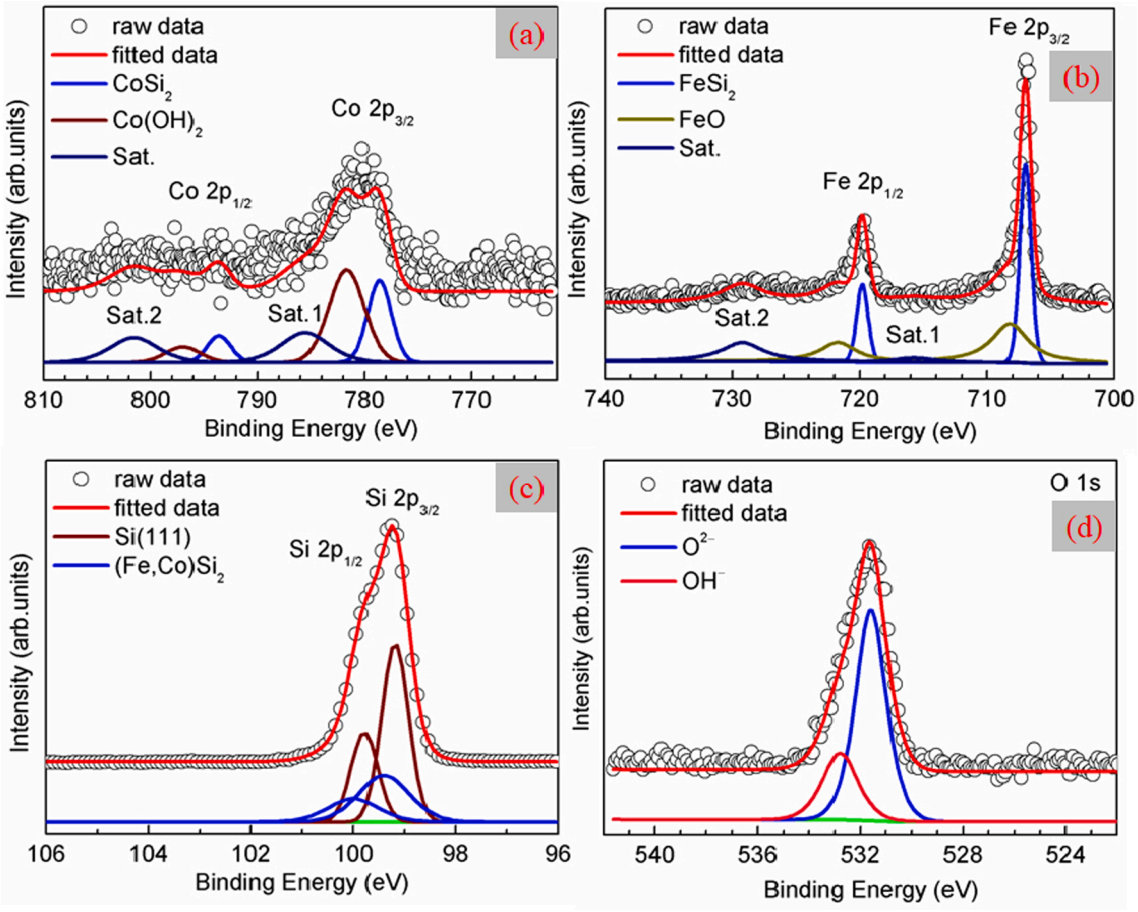

Fig. 7. The XPS data confirms the co-existence of $FeSi_2$ and $CoSi_2$ islands on the Si(1 1 1) surface.

di-silicides fabricated on the same Si(1 1 1)-7 × 7 surface may be utilized in the nanodevice fabrication. For ferromagnet-superconductor hybrid structure applications in quantum technology, it is important to control the separation between the ferromagnetic and the superconducting, in other words between $FeSi_2$ and $CoSi_2$, nanostructures on the substrate. This separation can be controlled via the amount of Fe and Co deposition.

CRediT authorship contribution statement

J.C. Mahato: Conceptualization, Methodology, Visualization, Investigation, Formal analysis, Writing – original draft. **Debolina Das:** Investigation, Formal analysis. **Arindam Pal:** Investigation, Formal analysis. **Prabir Pal:** Investigation, Formal analysis. **B.N. Dev:** Funding acquisition, Resources, Visualization, Supervision, Writing – review & editing.

Declaration of Competing Interest

The authors declare that they have no known competing financial interests or personal relationships that could have appeared to influence the work reported in this paper.

Acknowledgement

JCM and DD were supported by CSIR Fellowships [09/080(0674)/2009-EMR-I] and [09/080(0725)/2010-EMR-I] respectively. The work has been partially supported by the IBIQuS project (DAE OM No. 6/12/2009/BARC/R&D-I/50, Dated 01.4.2009). This work was carried out in BND's laboratory when JCM, DD, AP and BND were all at Indian Association for the Cultivation of Science, Kolkata, India.

References

[1] L.J. Chen, Metal Silicides: An Integral Part of Microelectronics, JOM 57 (2005) 24.
[2] V.S. Neshpor, J. Eng. Phys. 15 (1968) 750–752.
[3] F. Nava, K.N. Tu, O. Thomas, J.P. Senateur, R. Madar, A. Borghesi, G. Guizzetti, U. Gottlieb, O. Laborde, O. Bisi, Mater. Sci. Rep. 9 (1993) 141–200.
[4] S.P. Murarka, Intermetallics 3 (1995) 173–186.
[5] H. Hsu, W. Huang, T. Chen, et al., Nanoscale Res. Lett. 8 (2013) 224.
[6] Q. Wan, T.H. Wang, C.L. Lin, Appl. Phys. Lett. 82 (2003) 3224.
[7] G.I. Glushkov, A.V. Tuchin, S.V. Popov, L.A. Bityutskaya, Semiconductors 49 (2015) 1695–1697.
[8] D. Leong, M. Harry, K.J. Reeson, K.P. Homewood, Nature 387 (1997) 686.
[9] R. Imlau, A. Kovacs, E. Mehmedovic, P. Xu, A.A. Stewart, C. Leidinger, et al., Phys. Rev. B 89 (2014), 054104.
[10] D.Z. Chi, Thin Solid Films 537 (2013) 1–22.
[11] J.K. Tripathi, G. Markovich, I. Goldfarb, Appl. Phys. Lett. 102 (2013), 251604.
[12] J.K. Tripathi, R. Levy, Y. Camus, M. Dascalu, F. Cesura, R. Chalasani, A. Kohn, G. Markovich, I. Goldfarb, Appl. Surf. Sci. 391 (2017) 24–32.
[13] R. W. Fathauer, P. J. Grunthaner, T. L. lin, K. T. Chang, J. H. Mazu, D. N. Jamieson, J. Vacuum Sci. Technol. B: Microelectron. Process. Phenom. 6, 708 (1988).
[14] L. Dózsa, Š. Lányi, V. Raineri, F. Giannazzo, N.G. Galkin, Nanoscale Res. Lett. 6 (2011) 209.
[15] Y.L. Jiang, X.P. Qu, G.P. Ru, B.Z. Li, Appl. Phys. A 99 (2010) 93–98.
[16] Z. Zou, W. Li, J. Liang, D. Wang, Acta Materialia 59 (2011) 7473–7479.
[17] M.A.K. Zilani, H. Xu, X.S. Wang, A.T.S. Wee, Appl. Phys. Lett. 88 (2006), 023121.
[18] J.K. Tripathi, M. Garbrecht, W.D. Kaplan, G. Markovich, I. Goldfarb, Nanotechnology 23 (2012), 495603.
[19] V.S. Zhandun, N.G. Zamkova, S.G. Ovchinnikov, I.S. Sandalov, Phys. Rev. B 95 (2017), 054429.
[20] I. Goldfarb, Y. Camus, M. Dascalu, F. Cesura, R. Chalasani, A. Kohn, Phys. Rev. B 96 (2017), 045415.
[21] J.C. Mahato, D. Das, P. Das, T.K. Chini, B.N. Dev, Nano Express 1 (2020), 020045.
[22] B.L. Ong, S.W. Ong, E.S. Tok, Surf. Sci. 647 (2016) 84–89.
[23] B.T. Matthias, J.K. Hulm, Phys. Rev. 89 (1953) 439.
[24] B.W. Roberts, J. Phys. Chem. Ref. Data 5 (1976) 581.

[25] P. A. Badoz, A. Briggs, E. Rosencher and F. Arnaud d'Avitaya, J. Physique Lett., 46, L-979 L-983 (1985).
[26] S.P. Chiu, S.S. Yeh, C.J. Chiou, Y.C. Chou, J.J. Lin, C.C. Tsuei, ACS Nano 11 (1) (2017) 516–525.
[27] N. Onda, J. Henz, E. Mueller, K.A. Maeder and H. yon Kaenel, Appl. Surf. Sci., 56-58 421–426 (1992).
[28] S. Liang, R. Islam, D.J. Smith, P.A. Bennett, J.R. O'Brien, B. Taylor, Appl. Phys. Lett. 88 (2006), 113111.
[29] J. Desimoni and F.H. Śanchez, Hyperfine Interactions, 113, 403–410 (1998).
[30] Liwei D. Geng, Sahil Dhoka, Ilan Goldfarb, Ranjit Pati, Yongmei M. Jin, Origin of Magnetism in γ-$FeSi_2$/Si(111) Nanostructures, Nanomaterials 11 (4) (2021) 849, https://doi.org/10.3390/nano11040849.
[31] H. Mooij, Superconducting quantum bits – Physics World, 01 December, (2004).
[32] J.C. Mahato, D. Das, R. Batabyal, A. Roy, B.N. Dev, Surf. Sci. 620 (2014) 23–29.
[33] J.C. Mahato, D. Das, R.R. Juluri, R. Batabyal, A. Roy, P.V. Satyam, B.N. Dev, Appl. Phys. Lett. 100 (2012), 263117.
[34] J.C. Mahato, D. Das, N. Banu, B. Satpati, B.N. Dev, Nanotechnology 28 (2017), 425603.
[35] D. Das, J.C. Mahato, B. Bisi, B. Satpati, B.N. Dev, Appl. Phys. Lett. 105 (2014), 191606.
[36] I.F. Lyuksyutov, V.L. Pokrovsky, Adv. Phys. 54 (2005) 67–136.
[37] G. Kurizki, P Bertet, Y. Kubo, K. Mølmer, D. Petrosyan, P. Rabl, and J. Schmiedmayer, PNAS March, 112, 3866–3873 (2015).
[38] Y. Manassen, H. Realpe, R. Shneck, D. Barlam, A. Brokman, Phys. Rev. B 68 (2003), 075412.
[39] R.P. Brady, A.S. Sharma, R.L. Giblet, R.J. Cottier, T.D. Golding, J.M. Perez, Appl. Phys. Lett. 86 (2005), 223102.
[40] K. Kataoka, K. Hattori, Y. Miyatake, H. Daimon, Phys. Rev. B 74 (2006), 155406.
[41] A. Wawro, S. Suto, R. Czajka, A. Kasuya, Nanotechnology 19 (2008), 205706.
[42] D. Das, T. Choudhury, Bull. Mater. Sci. 43 (2020) 86.
[43] M. Krause, F. Blobner, L. Hammer, K. Heinz, U. Starke, Phys. Rev. B 68 (2003), 125306.
[44] R.P. Brady, A.S. Sharma, R.L. Giblet, R.J. Cottier, T.D. Golding, et al., Appl. Phys. Lett. 86 (2005), 223102.
[45] Z. He, D.J. Smith, P.A. Bennett, Phys. Rev. Lett. 93 (2004), 256102.
[46] L. Fernández, M. Löffler, J. Cordón, J.E. Ortega, Appl. Phys. Lett. 91 (2007), 263106.
[47] B.L. Ong, W. Ong, Y.L. Foo, J. Pan, E.S. Tok, Surf. Sci. 606 (2012) 1649–1669.
[48] J.C. Mahato, D. Das, A. Roy, R. Batabyal, R.R. Juluri, P.V. Satyam, B.N. Dev, Thin Solid Films 534 (2013) 296–300.
[49] B.L. Ong, E.S. Tok, Appl. Surf. Sci. 466 (2019) 583–591.
[50] K. Sekar, G. Kuri, P.V. Satyam, B. Sundarvel, D.P. Mahapatra, B.N. Dev, Surf. Sci. 339 (1995) 96.
[51] K. Sekar, P.V. Satyam, G. Kuri, B. Sundaravel, D.P. Mahapatra, B.N. Dev, Phys. Rev. B 51 (1995) 14330.
[52] B.W. Dodson, D.R. Myers, Phys. Rev. Lett. 61 (1988) 2681.
[53] T. Ghosh, P. Das, T.K. Chini, T. Ghosh, B. Satpati, Phys. Chem. Chem. Phys. 16 (2014) 16730.
[54] M.A. Visotin, I.A. Tarasov, A.S. Fedorov, S.N. Varnakov, S.G. Ovchinnikov, Acta Cryst. B76 (2020) 469–482.
[55] Jin Zhao, Derrick M. Poirier, Surf. Sci. Spectra 7 (2000) 329.
[56] Z.Q. Zou, L.M. Sun, G.M. Shi, X.Y. Liu, X. Li, Nanoscale Res. Lett. 8, Article number: 510 (2013).